Electrochimica Acta 576 (2026) 149649

Contents lists available at ScienceDirect

Electrochimica Acta

journal homepage: www.journals.elsevier.com/electrochimica-acta

Fully inkjet-printed poly(N-isopropylacrylamide)/graphene electrodes for electroanalytical sensing with pH switchable selectivity

Samuele Scotti, Andreas Lesch *

University of Bologna, Department of Industrial Chemistry "Toso Montanari", Via Piero Gobetti 85, Bologna, 40129, Italy

ARTICLE INFO

Keywords:
Inkjet printing
Hydrogel
Surface modification
Charged redox species
Electroanalysis

ABSTRACT

Fully inkjet-printed electrochemical sensors, based on a graphene electrode coated with cross-linked poly(N-isopropylacrylamide) (PNIPAAm), are presented. The PNIPAAm coating is realized by combined inkjet printing and simultaneous photopolymerization using an inkjet printer with integrated UV light source. The inkjet ink composition and printing parameters are both optimized to polymerize the PNIPAAm pre-cursors as rapid as inkjet printing, while guaranteeing at the same time the fulfilment of rheologic ink requirements, such as surface tension and viscosity. In order to achieve reproducible and homogeneous PNIPAAm coverage, the surface of the graphene electrode is modified by introducing cavities of an inkjet-printed dielectric grid. The electrochemical performance of the PNIPAAm/graphene electrodes is tested with standard redox couples of positive, neutral and negative charges. A filtering effect of negatively charged redox species in near neutral pH electrolyte solutions is obtained. PNIPAAm is a well-known thermo-responsive polymer, but the variation of solution and sensor temperature does not influence the filtering properties of the thin PNIPAAm hydrogel obtained herein by inkjet printing. A switching of the filter characteristics of the material is observed at pH 2, at which the PNIPAAm hydrogel becomes permeable for negatively charged and impermeable for positively charged redox species. Finally, the filtering characteristics of the PNIPAAm/graphene electrode are evaluated for the electrochemical detection of the positively charged analyte dopamine in the presence of the negatively charged interferent ascorbic acid.

1. Introduction

Electrode surface modification is a widely used method to improve the functionality of amperometric sensors. Amperometric sensors are electrochemical devices and electrodes, which record as a response to a potential pulse, as well as, to a potential scan, the Faradaic current, generated by one or more heterogeneous electron transfer reactions. The scope of electrode surface functionalization of amperometric sensors is very diverse. It ranges from improvements of general electrochemical phenomena, such as thermodynamics, kinetics (overpotential reduction), real (effective) surface area and mass transport characteristics, to more specialized effects that include selectivity, sensitivity and durability [1]. Selectivity is often realized by introducing biorecognition elements, *e.g.*, antibodies and aptamers. These receptors are frequently combined with mediators, either immobilized on the electrode surface or dissolved in solution, such as in electrochemical biosensors [2,3]. Alternatively, selectivity can be achieved by considering overpotentials and appropriate electrocatalysts [4,5], such as for enzyme-less glucose sensing [6,7]. In such cases, the target is to separate the overpotential of an analyte from those of the interferents. Another common surface functionalization approach is based on coating the electrode surface with polymeric layers, which can be membranes or hydrogels, or even layered clay minerals [8]. Very common are polymeric layers containing covalently bound redox mediators, known as redox polymers, that are frequently used in biosensors, such as those for glucose [9,10]. Polymers and co-polymers are used in order to implement one or more different functions to the initially bare amperometric electrode, in particular electrode surface protection and stabilization [11–13]. For instance, polyacrylamide (PAAm), also as co-polymer, is an often used hydrogel that can be obtained by chemical or photochemical polymerization of acrylamide with and without cross-linkers, such as N, N′-methylenebisacrylamide, and, optionally, co-monomers [14]. Polyacrylamide coatings on amperometric electrodes can reduce electrode contamination when the electrodes are used in complex matrices that are rich in electrode fouling species [15–18]. Polyacrylamide hydrogels can also be used to entrap and thus immobilize enzymes and proteins

* Corresponding author.
E-mail address: andreas.lesch@unibo.it (A. Lesch).

https://doi.org/10.1016/j.electacta.2026.149649
Received 17 March 2026; Received in revised form 11 July 2026; Accepted 1 August 2026
Available online 1 August 2026

close to the electrode surface as needed for biosensing [19]. In polyacrylamide hydrogels, especially when they are rather thick, the diffusion coefficients of redox-active species appear to be lower than in solution [20]. As a result, peak-to-peak separations of reversible and quasi-reversible redox couples increase while their respective peak currents decrease. However, when made thin the PAAm-coated electrodes respond with very little difference to their non-coated counterparts. Recently, PAAm hydrogels demonstrated significant pre-concentration of the analyte carbendazim for its detection, enhancing therefore significantly the sensor sensitivity [21]. Using acrylamide derivatives can significantly change the hydrogel characteristics and functionalities. For instance, replacing acrylamide by N-isopropylacrylamide results in Poly(N-isopropylacrylamide) (PNIPAAm), which is a well-known thermo-responsive hydrogel [22,23]. Below its lower critical solution temperature (LCST) of about 32 °C, PNIPAAm hydrogels are swollen with enlarged pores while above the LCST water is removed from PNIPAAm resulting in shrinking and pore size reduction. As a consequence, PNIPAAm hydrogels can be used as temperature-controlled filter for the transport of species in water [24,25]. In combination with electrochemical sensors, it has been reported in details how sensor performance can be switched with temperature [26–31].

Hydrogels based on acrylamide or common acrylate derivatives, and thus acrylic-based polymers in general, are attractive materials in terms of large scale fabrication abilities, in particular related to easiness and low cost. Thin hydrogel layers can principally be fabricated directly on an electrode surface by reactive screen printing or inkjet printing approaches, in which the hydrogel precursors, *i.e.*, the monomer(s) and cross-linker(s), are deposited in form of an ink or paste that is polymerized by means of photochemical, chemical or thermal approaches [32]. However, production challenges are faced in terms of ink stability, pattern resolution and rapid as well as complete polymerization. Inkjet printing of nanometer-thin hydrogel layers has been demonstrated by Lesch et al. for polyacrylamide-coated carbon nanotube electrodes [33]. The hydrogel layers were reproducible, stable and provided surprising matrix-elimination effects for the detection of antioxidants in wine and orange juice. The combination of inkjet printing of particle-free metal, metal oxide or polymer precursor inks with light-induced metal and metal oxide reduction or polymerization reactions is indeed a powerful approach towards stable low cost production of electrodes and devices in general [34,35].

In this work, the fabrication of fully inkjet-printed cross-linked PNIPAAm-coated graphene electrodes is presented. We present the formulation of the inks, the optimization of printing and a thorough electrochemical characterization of the electrodes for electroanalytical applications. Surprisingly, inkjet-printed PNIPAAm-coated graphene electrodes showed different blocking of charged redox species, which was dependent on pH. We demonstrate several efforts to try to understand the origin of this observation that to the best of our knowledge has not been reported elsewhere.

2. Experimental section

2.1. Materials

N-Isopropylacrylamide (NIPAAm, Acros Organics, 99% purity), acrylamide/N,N'Methylenebisacrylamide 37.5:1 (40%, Acros Organics), N,N'Methylenebisacrylamide (Alfa Aesar, >99%), Riboflavin (Sigma-Aldrich, ≥98%), N,N,N',N'-Tetramethylethylenediamine (TEMED, Sigma-Aldrich, 99%), Triton™ X-100 (Sigma-Aldrich), potassium hexacyanoferrate ($K_3[Fe^{III}(CN)_6]$, Riedel-de Haën, puriss. p.a.), ferrocenemethanol (FcMeOH, Sigma-Aldrich, 97%), hexaammine ruthenium chloride ($[Ru^{III}(NH_3)_6]Cl_3$, Sigma-Aldrich, 98%), L-ascorbic acid (Sigma-Aldrich, 99%), potassium nitrate (KNO_3, Sigma-Aldrich, ≥99%) and potassium phosphate monobasic (KH_2PO_4, Sigma-Aldrich, ≥99%) were used as received. DI water was produced by using an ionic exchange resin filter. The pH of solutions was measured by using an AMEL Instrument 338 pH meter.

Polyimide (PI) sheets (150 µm thickness) were obtained from Dr. Dietrich Müller GmbH (Germany) and served as substrates for inkjet printing. A graphene dispersion (graphene ink for inkjet printing with ethyl cellulose in cyclohexanone and terpineol, Sigma-Aldrich) and SunTronic UV curing jettable insulator ink (Sigma-Aldrich) were used as commercial inkjet inks and used as received.

2.2. Ink formulation and inkjet printing

Stock solutions of 12% (w/v) NIPAAm/MBIS with 2.6% C and riboflavin (77 mg/L) were prepared in DI water. Different ratios of the stock solutions and different additions of TEMED have been tested for the pre-polymerization step, specifically developed and applied i) to increase the ink viscosity to values necessary for inkjet printing and ii) to obtain with simultaneous UV photopolymerization the full hydrogel film just within the printing time. The pre-polymerization was carried out in a glass vial under stirring (stirring rates were varied between 600 rpm and 1500 rpm), using the OmniCure S2000 Spot UV Curing System (Excelitas, 200 Watt). The lamp outputs were up to 30 W/cm^2 and regulated by changing the UV lamp iris level between 1% and 3%. It must be noted that the pre-polymerization step depends on vial diameter, distance as well as position of the light source, and the type and dimension of the stirrer bar as well as the stirrer rotation rate. Ink composition details are given in the results section. The ink viscosities and surface tensions were measured using a viscometer SV-1A (A&D Weighing, Japan) and the Dropometer pendant droplet analyzer (Droplet Lab, Canada). The polymerization of the ink components for hydrogel formation is furthermore influenced by oxygen acting as scavenger, thus lowering the process efficiency. However, all procedures were carried out under ambient atmosphere. The inks for PAAm printing were prepared as described in detail in our previous work [33].

A Dimatix Materials Printer DMP-2831 (Fujifilm) was used for drop-on-demand inkjet printing. The UV light from the Omnicure lamp was transferred into the printer by using a liquid UV light guide, whose opening (the output diameter was 5 mm) was mounted next to the printhead using a customized holder. This enabled quasi-simultaneous inkjet printing and light irradiation of the as-deposited ink. For inkjet printing, DMC-11610 cartridges (Fujifilm Dimatix) were employed, which operate under piezoelectric actuation. With these printheads, nominal droplet volumes of 10 pL are generated using up to 16 individually addressable nozzles. As conductive electrode support layer, the commercial graphene ink was printed and thermally cured at 400 °C for 30 min using a heating ramp of 2 °C/min in a Thermolyne (ThermoFisher scientific) muffle furnace. The UV curable dielectric ink was printed and quasi-simultaneously photo-polymerized into a well-defined insulation pattern in order to determine the active, geometric electrode area and to deposit an insulating grid on the WE surface with the aim to obtain more homogeneous hydrogel layers (*vide infra*). Conventional inkjet printing parameters, such as the piezoelectric actuation pulse and jetting frequency, were optimized for each ink (graphene, UV photopolymerizable hydrogel precursor and UV curable insulator inks). For hydrogel and insulation layer inkjet printing, the maximum UV lamp intensity was used.

2.3. Characterizations of the electrodes

A Leitz Laborlux D (Leitz) in combination with conventional smartphone cameras and a digital microscope model AM4133T (Dino-Lite) were employed for the visual inspection of the electrodes.

Electrochemical measurements, *i.e.*, cyclic voltammetry, were carried out using a potentiostat VersaSTAT 3F (Ametek – Princeton Applied Research) and a CHI-900 potentiostat (CH Instruments). Bare graphene electrodes and graphene electrodes coated with PNIPAAm or PAAm were used as working electrodes (WEs) in a conventional three electrode

arrangement. Either a saturated calomel electrode (SCE) or a Ag/AgCl/1 M KCl electrode was used as reference electrode (RE) and a platinized platinum mesh with significantly larger surface area compared to the WE was used as counter electrode (CE). All potentials herein are referred to these REs as stated in the figure captions. All measurements were carried out without compensating the uncompensated resistance and CV data are shown as measured. The distance between the electrodes was about 1 cm.

3. Results

3.1. Inkjet printing of the gel-coated electrodes

In order to print PNIPAAm hydrogels by using inkjet printing, the ink composition was optimized with the prior aim to identify the proper concentrations and ratios of all ingredients for both their rapid and complete photopolymerization and to fulfil the rheologic requirements for inkjet printing. The latter addresses in particular the ink viscosity and surface tension. The ideal ink composition contains the hydrogel monomer, cross-linker, catalyst and photo-initiator, using just water as solvent. As it had been demonstrated in our earlier works, the addition of a certain amount of pre-synthesized polymer to the ink increases ink viscosity, but hinders rapid photopolymerization. In such cases, printed patterns are not fully polymerized and cross-linked so that they dissolve when immersed in solution. Therefore, we followed the approach of a two step inkjet ink synthesis, which was based on the initial preparation of a solution containing reduced amounts of photoinitiator and catalyst, but already the final amounts of monomer and cross-linker. With this pre-ink a controlled pre-polymerization step can be performed. In this way, individual PNIPAAm particles were generated increasing the ink viscosity from 0.9 mPa s (not printable) to about 1.8 mPa s (printable). This was achieved by adding for instance to 4 mL of the 12% (w/v) NIPAAM/MBIS with 2.6% C stock solution 90 μL of the Riboflavin stock solution and 7.5 μL of TEMED. For inkjet printing, the surface tension was decreased from 70 mN/m (not printable) to about 30 mN/m (printable) by adding to the pre-polymerized ink a little amount of Triton-X, *i.e.*, 2.4 μL. Additional catalyst (20 μL of TEMED) and photo-initiator (600 μL of the Riboflavin stock solution) were then added to the pre-polymerized ink in increased quantities, in order to realize rapid "final" photopolymerization simultaneously to printing, thus the complete formation of the hydrogel layer on the target substrate. The scope of this work was to polymerize the hydrogel precursors with a yield as close as possible to 100%. Successful polymerization was rapidly verified by comparing the hydrogel patterns as-printed before and after immersion into water. In case of incomplete or partial polymerization the hydrogel pattern dissolved entirely or in part and was, consequently, not usable as electrode modification layer. Microscopic hydrogel instabilities were tested electrochemically (*vide infra*). The substrates for hydrogel printing were inkjet-printed graphene electrodes on polyimide foils (Fig. 1a and b). The active graphene electrode area was defined by simultaneous inkjet printing and photopolymerization of a UV curable dielectric ink, which generated a solid, solution impermeable insulator. The active geometric area of the bare graphene electrodes was generally about 1 mm^2. Differently to our previous PAAm inkjet printing works, PNIPAAm did not generate a homogeneous hydrogel layer on the graphene pattern, even after printing six inkjet printed layers (IJPLs) (Fig. 1c). Several zones of the graphene area remained uncoated, while others were coated with excess of PNIPAAm. This suggests that there was a clear mismatch between graphene surface and ink/polymer characteristics, resulting in an unfavourable ink-substrate interaction. As demonstrated in a previous work [36], the graphene electrode is relatively hydrophilic due to the presence of ink stabilizing agents, while the formation of PNIPAAm under UV light exposure seemed to generate a hydrophobic polymer layer. In order to obtain full coverage of the graphene electrode, 12 IJPLs had to be printed, generating however still relative inhomogeneous hydrogel patterns. Nevertheless, the

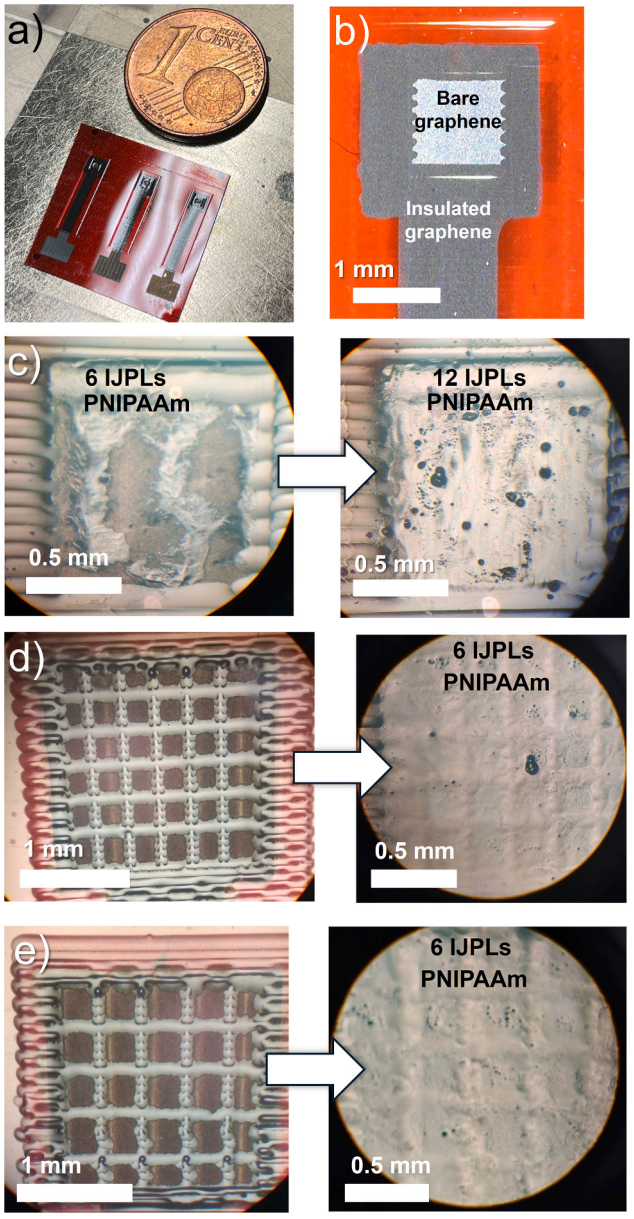

Fig. 1. a) Three fully inkjet-printed graphene electrodes with insulation layer and PNIPAAm hydrogel layer on polyimide with size comparison to a 1 Euro Cent coin. b) Detailed view on the active surface before hydrogel printing, *i.e.*, the bare graphene "window" to be coated. c) 1 mm^2 graphene electrode coated with 6 IJPLs (left panel) and 12 IJPLs (right panel) of PNIPAAm hydrogel. d) Grid-coated graphene electrode (graphene array units of 185 μm × 170 μm size) before (left panel) and after (right panel) deposition of 6 IJPLs of PNIPAAm hydrogel. e) Grid-coated graphene electrode (graphene array units of 305 μm × 235 μm) before (left panel) and after (right panel) deposition of 6 IJPLs of PNIPAAm hydrogel.

PNIPAAm/G electrodes can be individually re-used and analyses can be performed by repetitive one-sensor measurements (*vide infra*). However, in case of disposable use for monitoring or calibration measurements in complex matrices, electrode production must be made more reproducible. In order to reach reproducibly a homogeneous PNIPAAm layer, the electrode dimension was first reduced to a smaller circle (Supporting Information SI-1). However, this approach was unsuccessful. Thereafter, a larger bare graphene electrode was first covered with a grid of insulator, forming an array of smaller squared bare graphene patterns, appearing as cavities (185 μm × 170 μm and 305 μm × 235 μm, respectively). This approach turned out to be successful, as much more

homogeneous PNIPAAm hydrogel layers on graphene were obtained (Fig. 1d and e). By the implementation of the grid cavities, the spreading of the polymerizing ink was reduced, generating hole-free PNIPAAm patterns and thus a much more effective coating. The thicknesses of inkjet-printed hydrogel layers, such as the previously reported PAAm and the herein presented PNIPAAm layers, generally range from nanometers to very few micrometers for one printed pattern and 2 IJPLs [33]. In line with this, the PNIPAAm layers shown in Fig. 1d and e demonstrated thicknesses between ~1 μm and ~14 μm for a single electrode with 6 IJPLs (SI-2). This thickness variation can be explained by the ink spreading and polymerization dynamics on the graphene surface inside the polymer grid cavities as described above.

3.2. Electrochemical performance of the gel-coated electrodes

Thereafter, the as-printed PNIPAAm/G electrodes were tested for their electrochemical properties, in particular to evaluate whether and how the hydrogel layer affects the shape of CVs using standard electro-active species in aqueous electrolytes. CVs were first recorded in 0.1 M KNO_3 solution containing either $[Fe(CN)_6]^{3-}$ or FcMeOH as typical redox species for the amperometric characterization of the electrodes. The analyte concentration was in both cases 1 mM. The bare graphene electrode showed the typical redox peaks of these redox species, as expected for this inkjet-printed thin film graphene electrode, deposited without underlying conductive support layers on a plastic foil (Fig. 2a). For $[Fe(CN)_6]^{3-}$, the electrode kinetics were rather slow, while for FcMeOH they appeared much faster, even though the same WE electrode material was used. In addition, the currents recorded with the bare graphene electrode showed a noticeable capacitive contribution, in line with what we reported previously [36]. In fact, the characteristics of the inkjet-printed bare graphene electrodes, and the negative and positive influences of various fabrication process parameters, such as thermal treatments post-printing, have been discussed in detail in our previous work [36]. The commercial graphene ink contained as a second important component, apart from graphene, which was ethyl cellulose. Ethyl cellulose acted on the one hand as an ink stabilizer. On the other hand, after thermal treatment of the printed ink patterns, ethyl cellulose degraded and converted into a binder, stabilizing the graphene layer and promoting adhesion to the plastic support. As a secondary effect, the electrochemical properties, such as capacitive currents and slowed electrode kinetics for electro-active species, in particular for $[Fe(CN)_6]^{3-}$, were compromised. The CVs for $[Fe(CN)_6]^{3-}$, recorded with PNIPAAm/G electrodes, did not show redox peaks, but capacitive currents of similar intensity as for the non-coated graphene electrode. The presence of similar capacitive currents suggests that the hydrogel layer did not insulate the graphene electrode surface underneath and that graphene was in contact with the electrolyte solution. In fact, when using FcMeOH, for both the coated and non-coated graphene electrodes the redox peaks were clearly observed, indicating a quasi-reversible system (Fig. 2b). The reduction peak for $FcMeOH^+$ in the reverse scan was reduced, as a result of the graphene electrode characteristics, as previously analyzed and reported [36]. The two peak currents for bare graphene were slightly higher and the two peak potentials closer on the bare graphene electrode compared to the PNIPAAm/G electrode, indicating a slightly sacrificed graphene electrode performance in presence of the hydrogel. This might be explained by slower diffusional mass transport inside the PNIPAAm coating and superimposed reduced electrode kinetics. Comparing both redox couples, *i.e.*, $[Fe(CN)_6]^{3-/4-}$ and $FcMeOH^{+/0}$ using the PNIPAAm/G electrodes (Fig. 2c), it is evident that $[Fe(CN)_6]^{3-/4-}$ became undetectable when using the same CV parameters. One reason could be significantly reduced electrode kinetics, but as the redox peaks entirely disappeared when adding the hydrogel, another redox species-selective exclusion mechanism should be dominant. Indeed, the negatively charged redox couple $[Fe(CN)_6]^{3-/4-}$ seems to be blocked from reaching the graphene electrode surface by processes occurring inside the several micrometer thick PNIPAAm layer or at the graphene-PNIPAAm interface. For the $FcMeOH^{+/0}$ redox couple, the electrode surface was accessible. Indeed, as discussed *vide infra*, the $[Fe(CN)_6]^{3-/4-}$ redox peaks start to appear at the expected potentials (*i.e.*, similar to the ones for bare graphene) when the hydrogel is immersed for extended times in solution, suggesting that the reason of the observations is mass transport-based and not kinetically driven.

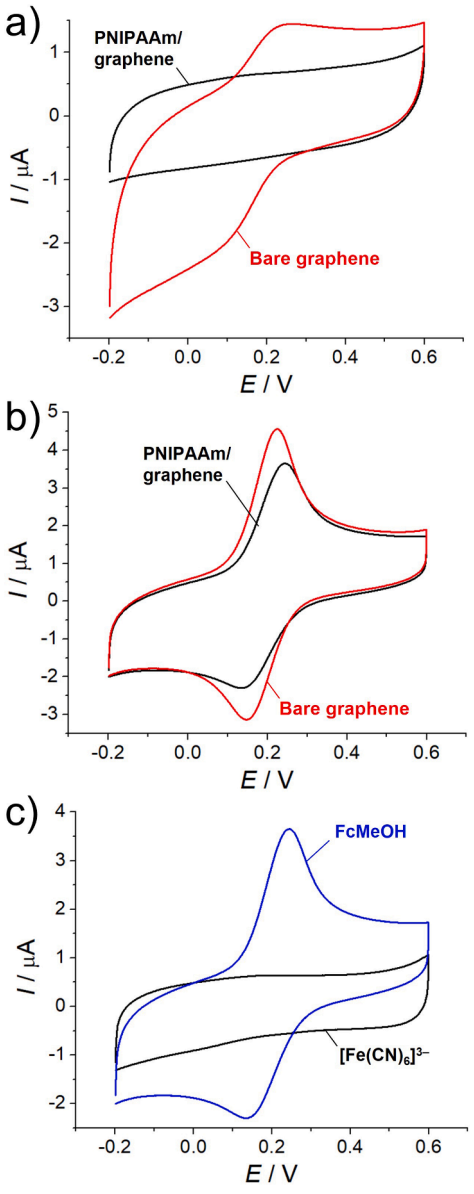

Fig. 2. CV shape comparisons with 1 mM of two different electro-active species in 0.1 M KNO_3 using PNIPAAm/graphene and bare graphene inkjet-printed electrodes. a) $[Fe(CN)_6]^{3-}$ for PNIPAAm/graphene electrode (Grid-2, 6 IJPLs; black curve) and bare graphene electrode (red). b) FcMeOH for PNIPAAm/graphene electrode (no grid, 12 IJPLs; black) and bare graphene electrode (red). c) Direct analyte comparison: $[Fe(CN)_6]^{3-}$ (black) and FcMeOH (blue) for two PNIPAAm/graphene electrodes from (a) and (b). RE: SCE.

Before going more into mechanistic details, the general performance of the PNIPAAm/G electrode during electrochemical measurements was evaluated. The hydrogel-coated electrodes could be used as printed or after storing at air. This demonstrates that the hydrogel layer exhibits immediate permeability for the redox species of interest once the hydrogel-coated electrodes have been immersed into the solution. However, a dried PNIPAAm/G electrode required some minutes to swell until a steady-state behaviour was reached (SI-3). Once the steady-state

swelling was reached, the PNIPAAm/G electrode response was relatively stable over time. However, with extended immersion times, the swollen hydrogel started to become slightly permeable for $[Fe(CN)_6]^{3-/4-}$. Indeed, the appearance of small, but slightly increasing redox peaks for the $[Fe(CN)_6]^{3-/4-}$ redox couple was observed after 10 and 20 CV cycles, respectively, while total analyte blocking was achieved with the dry PNIPAAm/G electrode (SI-4). This could have been caused by continuous hydrogel swelling, extending the hydrogel pores and enabling also the mass transport of initially non-favoured species. However, the inkjet-printed PNIPAAm/G electrodes are considered for rapid and disposable use, thus not for usage over extended time periods in solution. This minor peak appearance over time is herein reported for the sole purpose of providing a complete sensor performance characterization. Furthermore, the PNIPAAm hydrogel did not detach from the graphene surface, as the hydrogel appearance on graphene before and after tests in solution was the same, and as electrodes could be reused without noticed limitations.

Thereafter, the electrochemical detection of $[Fe(CN)_6]^{3-}$ for the PNIPAAm/G electrode was compared with the results obtained using a PAAm/G electrode. This means that the monomer N-isopropylacrylamide of PNIPAAm was replaced by acrylamide (AAm) to generate PAAm. All other hydrogel and inkjet ink components were kept the same. The primary amide of acrylamide is converted into a secondary amide in N-isopropylacrylamide where one H was replaced by an isopropyl group. This substitution induces hydrophobic properties in PNIPAAm. However, whether and how much this change in hydrophobicity contributes to the observed selectivity for electroanalysis, which indeed was not observed for PAAm, remains so far unclear. As it can be seen clearly from the CVs, polyacrylamide did not block $[Fe(CN)_6]^{3-}$ (Fig. 3a). For the PAAm/G electrode, the redox peaks are clearly visible. However, the CV does not represent a reversible system due to the slow graphene electrode kinetics as discussed *vide supra*.

PNIPAAm is a well-known thermo-responsive polymer so that PNIPAAm hydrogels are often used as switchable filters for dissolved electro-active species. When operated at solution temperatures above the Lower Critical Solution Temperature (LCST), *i.e.*, 32–34 °C. the material expels water, shrinks and reduces its hydrophilic characteristics. In such state, the material in general blocks redox species. Cooling the PNIPAAm layer in solution below the LCST, the hydrogel turns back into its original structure by the uptake of water and switches to a more hydrophilic hydrogel. In that condition, redox species can pass better the PNIPAAm layer. Reversible swelling and compressing was also observed for the macroscopic version of the PNIPAAm hydrogel in this work, prepared by bulk synthesis in a vial instead of using the thin film synthesis with inkjet printing (SI-5). All ingredients remained identical for the bulk synthesis. In order to exclude that temperature-controlled swelling and compressing affects the electrochemical performance of the PNIPAAm/G electrodes of this work, experiments were carried out at different solution temperatures. Fig. 3b shows three CVs using one PNIPAAm/G electrode in the same electrolyte containing 1 mM $[Fe(CN)_6]^{3-}$ at two different temperature regimes: below the LCST (*i.e.*, RT and 4 °C) and above the LCST (80 °C). Relevant signal changes were not observed, suggesting that the well-known swelling/shrinking of the PNIPAAm hydrogel did not occur or did not have an impact on the electrochemical performance for the thin film PNIPAAm/G electrodes. Therefore, it might be that the PNIPAAm layer was too thin for inducing the different levels of swelling, well known for bulk PNIPAAm. Therefore, the PNIPAAm material synthesized herein behaved in bulk form as reported in the literature and as expected, but it showed different characteristics when printed as a thin layer on graphene.

PNIPAAm is known to be a non-ionic polymer without ionizable groups (*i.e.*, a neutral polymer). However, it was decided to acidify the solution and thus to reduce the solution pH. The electrolyte was changed from 0.1 M KNO_3 to phosphate buffered solutions. It was noticed, that at a solution pH of 3.5, the redox peaks for $[Fe(CN)_6]^{3-/4-}$ started to appear (Fig. 4a). Reducing the pH further, *i.e.*, to pH 2, the redox peaks for $[Fe(CN)_6]^{3-/4-}$ clearly appeared (Fig. 4b), suggesting that a change from 0.1 M KNO_3 to phosphate buffered solution with pH 2 caused a change inside the thin layer PNIPAAm layer or at its interfaces with graphene or the electrolyte solution. At pH 2, $[Fe(CN)_6]^{3-/4-}$ eventually reached the graphene electrode surface and became detectable. Moreover, compared to bare graphene, the electrode kinetics appeared much faster for the PNIPAAm/G electrode in phosphate buffered solution at pH 2, because the two redox peaks were much closer to each other and much better resolved compared to bare graphene (Fig. 4c). Thereafter, a positively charged electro-active species, *i.e.*, 1 mM $[Ru(NH_3)_6]^{3+}$ was selected for CV analysis. In 0.1 M KNO_3, the redox peaks for ruthenium$^{III/II}$ were clearly observable. The relatively slow electrode kinetics for the graphene electrode used herein has been reported elsewhere [36]. At pH 2, however, $[Ru(NH_3)_6]^{2+/3+}$ became undetectable (Fig. 4d). Reducing the solution pH, in general, can protonate protonable groups and generate a positively charged electrode surface. At pH 2, a positive surface charge could have electrostatically blocked the positively charged redox species, thus $[Ru(NH_3)_6]^{3+}$, and attracted the negatively charged ones, *i.e.*, $[Fe(CN)_6]^{3-/4-}$, instead. However, to the best of our knowledge, this effect is unusual for PNIPAAm, as the material does not contain protonable groups. In the literature, only in case of co-polymers, where for instance the ionizable co-monomer acrylic acid is introduced, surface charge effects are understandable [37]. At pH 2, in the PNIPAAm layer, the secondary amide group might have been slightly protonated as previously reported for poly(N-isopropylmethacrylamide) [38]. However, the origin of the observed analyte selectivity remains unclear at this point.

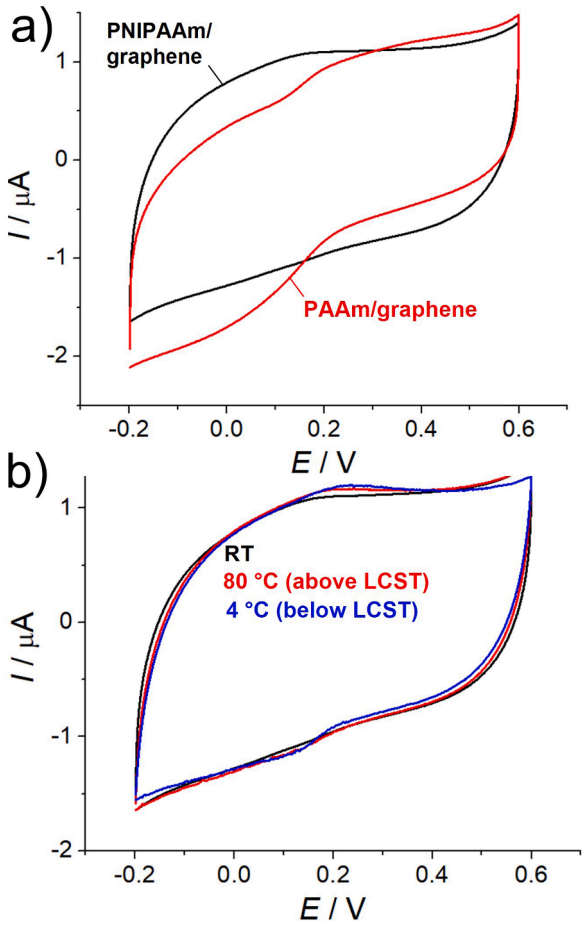

Fig. 3. CVs in 1 mM $[Fe(CN)_6]^{3-}$ and 0.1 M KNO_3. Scan rate 100 mV/s. a) Comparison of a PNIPAAm/graphene electrode (Grid-3, 6 IJPLs; black curve) with a PAAm/graphene electrode (red). b) One PNIPAAm/graphene electrode (Grid-3, 6 IJPLs) at different hydrogel temperatures: RT (black), 80 °C (red) and 4 °C (blue). RE: SCE.

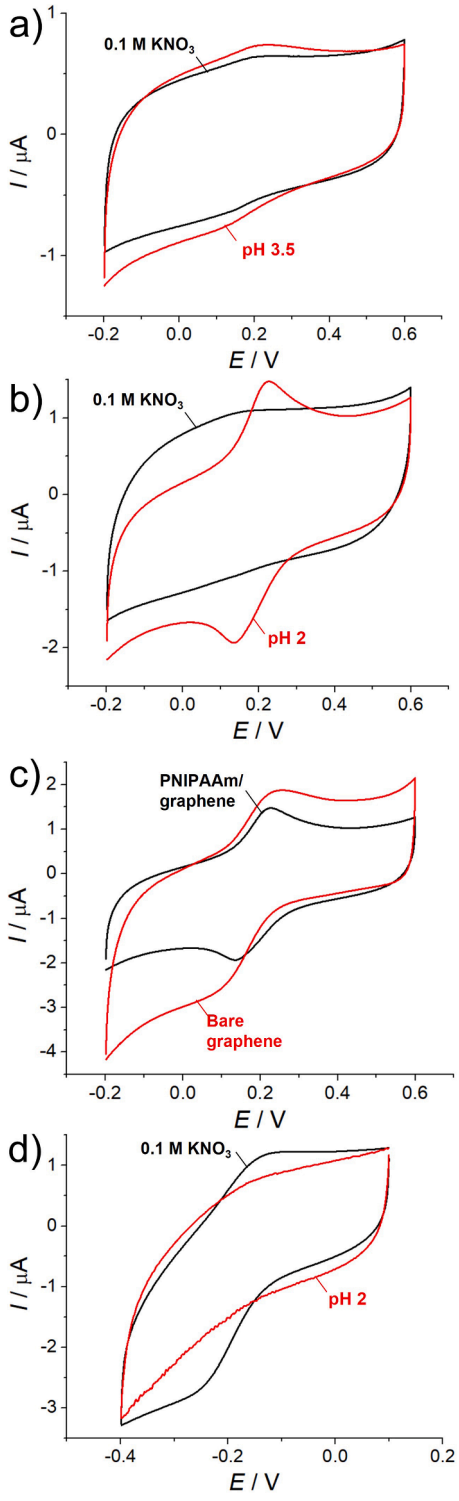

Fig. 4. CVs at different pH values. Scan rate 100 mV/s. a) 1 mM $[Fe(CN)_6]^{3-}$ in 0.1 M KNO_3 (black curve) and in PB pH 3.5 (red) using one PNIPAAm/graphene electrode (no grid). b) 1 mM $[Fe(CN)_6]^{3-}$ in 0.1 M KNO_3 (black curve) and in PB pH 2 (red) using two different PNIPAAm/graphene electrodes (Grid-3, 6 IJPLs). c) $[Fe(CN)_6]^{3-}$ detection in PB pH 2 for one PNIPAAm/graphene electrode (Grid-3, 6 IJPLs; black) and one bare graphene electrode (Grid-3; red). d) 1 mM $[Ru(NH_3)_6]^{3+}$ in 0.1 M KNO_3 (black curve) and in PB pH 2 (red) using one PNIPAAm/graphene electrode (no grid, 12 IJPLs). RE: SCE.

3.3. Application example: filtering of ascorbate as potential interferent in physiological solutions

A typical interferent during the detection of analytes in physiological solutions is ascorbic acid. Therefore, it was evaluated whether the inkjet-printed PNIPAAm/G electrode can eliminate or reduce signal contributions from ascorbic acid during the electrochemical determination of analytes. At physiological pH, *i.e.*, 7.4, ascorbic acid (pKa = 4.1–4.2) is present in solution mainly in its deprotonated, negatively charged form, hence as the ascorbate anion. Ascorbate is often present as an interferent in relevant concentrations and causes overlapping analytical signals. Generally, ascorbate is electro-oxidised at relative low potentials compared to biologically relevant redox species to be detected.

Instead of developing complicated biosensors or sample pretreatment methods to separate the analyte from the solution matrix and/or from ascorbate, it could be interesting and promising to introduce a simple-to-realize ascorbate filter, such as the thin film PNIPAAm. In line with the observations and assumptions made *vide supra*, 5 mM of the negatively charged ascorbate ion was hardly detectable at pH 7.4 using the inkjet-printed PNIPAAm/G electrode (Fig. 5a). Compared with the PNIPAAm-free graphene electrode, the signal suppression of ascorbate by the PNIPAAm layer is clearly evident (Fig. 5a). It must be noted, in line with the discussions in the previous section, that hydrated PNIPAAm seems to block a bit less efficiently the ascorbate ion (details in SI-6). However, the PNIPAAm-modified graphene electrode can offer new opportunities for the selective electrochemical detection of neutral and/or positively charged species, which are present in solutions of nearly neutral or slightly acidic pH. One typical analyte of general interest, which is also often used as a model analyte, is dopamine. Due to similar electro-oxidation potentials, dopamine itself or the signal for dopamine detection must be separated from ascorbate. The primary amine of dopamine has a pKa of ~8.9, thus at pH 7.4 dopamine will majorly be present as cation and should therefore pass the PNIPAAm layer. To verify this hypothesis, dopamine was added to the PB solution with 5 mM ascorbate to reach a dopamine concentration of 1 mM. As a result, and as expected, a clear oxidative wave correlated to the presence of dopamine was seen in the CV in Fig. 5b. The figure shows the CVs for the same PNIPAAm/G electrode in the analyte-free PB solution, the CV after adding ascorbate and then the CV after adding also dopamine. For comparison, a PB solution with only 1 mM dopamine was analysed and as well added to the graph. The blocking effect of the PNIPAAm layer for ascorbate was already described and is here clearly seen again. However, the current increased more than expected for a mixture of ascorbate and dopamine. Even though ascorbate was nearly completely blocked, the oxidation currents for dopamine in the ascorbate-dopamine mixture were significantly higher than for a solution of dopamine alone and for summing up the oxidative waves of the individual ascorbate and dopamine solutions (Fig. 5b, further details in SI-6). The second oxidation peak for dopamine (very weak in ascorbate-free solution) is much more pronounced. This suggests that ascorbate could have acted as a mediator for dopamine regeneration. Ascorbate could chemically react with the oxidized form of dopamine reducing the oxidized form of dopamine back to dopamine. As a consequence, the increased local availability of dopamine can result in higher currents and thus into signal enhancement. Following this strategy, indeed, there could be the possibility to detect ascorbic acid on demand, without changing the solution pH for thin film PNIPAAm switching, and without changing the protonation degree and thus the charge of ascorbic acid. Optionally, a redox mediator for ascorbate detection, such as FcMeOH, can be added [39,40]. FcMeOH is electro-oxidized at lower potentials than ascorbate, and, as demonstrated *vide supra*, passes the thin film PNIPAAm and reaches efficiently the electrode surface. FcMeOH is further known for the fact that its oxidized form $FcMeOH^+$ is rapidly reduced back to FcMeOH by ascorbate causing a positive effect for anodic ascorbate detection (1 mM), even though ascorbate does not reach the electrode

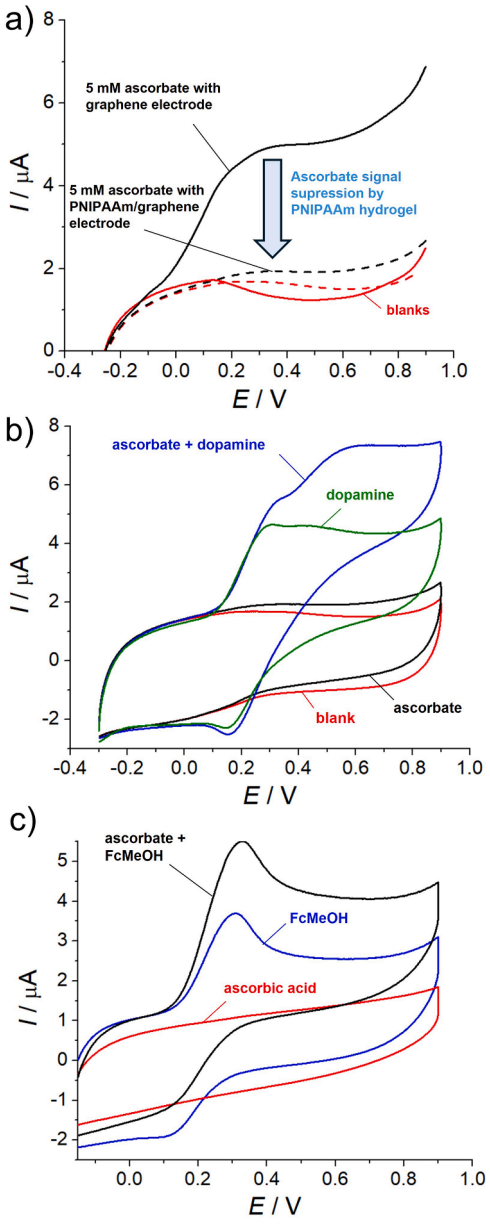

Fig. 5. a) Reduction of the interference of 5 mM ascorbic acid for the detection of 1 mM dopamine using a hydrated PNIPAAm/graphene electrode (Grid-3, 6 IJPLs). Comparison of PNIPAAm-coated (dashed lines, Grid-3, 6 IJPLs) and non-coated (solid lines, Grid-3) graphene electrodes in PB (pH 7.4) solutions in presence (black curves) and in absence (red curves, blanks) of 5 mM ascorbate. b) Detection of dopamine in presence of ascorbic acid using one hydrated PNIPAAm/graphene electrode (Grid-3, 6 IJPLs). 1 mM dopamine and 5 mM ascorbic acid in PB with pH 7.4 (blue curve), 5 mM ascorbic acid in PB with pH 7.4 (black), only PB with pH 7.4 (red) and 1 mM dopamine in PB with pH 7.4 (green). c) Switching between the elimination and FcMeOH-mediated detection of 1 mM ascorbic acid under physiological pH (*i.e.*, 7.4), using a PNIPAAm/graphene electrode (Grid-2, 6 IJPLs). 1 mM ascorbic acid + 1 mM FcMeOH in PB with pH 7.4 (black curve) in comparison to 1 mM ascorbic acid in PB with pH 7.4 (red) and 1 mM FcMeOH in PB with pH 7.4 (blue). Scan rate in all cases 100 mV/s. RE in (a) and (b): Ag/AgCl/1 M KCl. RE in (c): SCE.

surface due to its blocking by the PNIPAAm layer at pH 7.4 (Fig. 5c).

4. Conclusions

To conclude, graphene electrode modification with ultrathin layers of a cross-linked PNIPAAm hydrogel through inkjet printing has been presented. PNIPAAm inkjet printing has been realized by adopting a photopolymerization approach using N-isopropylacrylamide as monomer, N,N′-methylene bisacrylamide (bis-acrylamide) as cross-linker, TEMED as catalyst and riboflavin as photoinitiator. First, the ink composition was modified in order to obtain a stable and rapid inkjet printing process. While the surface tension could be decreased using a small addition of a surfactant, the viscosity was increased by performing a well-controlled, limited pre-polymerization to increase the ink viscosity to the printable range. With the optimized ink, and optimized printing parameters, hydrogel formation was as fast as inkjet printing. However, inkjet printing under parallel UV light irradiation resulted in the shrinking of the PNIPAAm thin film during printing and an inhomogeneous surface coverage of the graphene electrode underneath was the outcome. Hydrogel stabilizing, fully inkjet-printed acrylate-based polymer grids eventually enabled the printed PNIPAAm thin film layers to be reproducible and homogeneous. The PNIPAAm/G electrodes were ready-to-use and demonstrated remarkable electrochemical stability during voltammetric testing in solution. Interestingly, switchable pH dependent filtering of charged electro-active species was observed, which, to the best of our knowledge, has not been reported elsewhere previously. The negatively charged ferri-/ferrocyanide redox couple has been blocked by the PNIPAAm thin layer at near neutral pH values, while the hydrogel responded well, even better than bare graphene, to the ferri-/ferrocyanide redox couple at pH 2. The opposite was observed for positively charged redox species, such as the ruthenium hexaammine cation, which was detectable at near neutral pH, but became invisible to the electrode at pH 2. This suggests that the inkjet-printed cross-linked PNIPAAm thin film undergoes switching of their surface charges to cause repulsion or attraction of oppositely charged redox species, respectively, even though this is unexpected for PNIPAAm without combination with pH-responsive co-polymers. Finally, it was demonstrated how the PNIPAAm/G electrodes might be operated for the filtering at physiological pH of the ascorbate anion, a well-known interfering antioxidant anion. This work demonstrates how inkjet printing of classical materials in new forms and dimensions can lead to the discovery of new electrode functionalities, even though the mechanistic origin has yet to be disentangled. PNIPAAm is a well-known thermo-responsive hydrogel that can be switched between permeability and blocking based on solution temperature. It was tested and excluded that the thermosensitivity of PNIPAAm had an influence on the results. The observations presented herein suggest the possibility to use the inkjet-printed PNIPAAm thin layers for electroanalytical applications where filtering of charged species is a major requirement, in particular to eliminate the influence of interfering ions, typically present in complex matrices, such as food and beverages, for the final analytical applications.

CRediT authorship contribution statement

Samuele Scotti: Data curation, Investigation, Methodology. **Andreas Lesch:** Conceptualization, Methodology, Resources, Supervision, Validation, Writing – original draft, Writing – review & editing.

Declaration of competing interest

The authors declare that they have no known competing financial interests or personal relationships that could have appeared to influence the work reported in this paper.

Supplementary materials

Supplementary material associated with this article can be found, in the online version, at doi:10.1016/j.electacta.2026.149649.

Data availability

Data will be made available on request.

References

[1] R. Singh, R. Gupta, D. Bansal, R. Bhateria, M. Sharma, A Review on Recent Trends and Future Developments in Electrochemical Sensing, ACS Omega, 2023, https://doi.org/10.1021/acsomega.3c08060.

[2] Y. Zhu, M. Jović, A. Lesch, L. Tissières Lovey, M. Prudent, H. Pick, H.H. Girault, Immuno-affinity amperometric detection of bacterial infections, Angewand. Chem. - Int. Ed. 57 (2018) 14942–14946, https://doi.org/10.1002/anie.201808666.

[3] X. Wei, V.S. Reddy, S. Gao, X. Zhai, Z. Li, J. Shi, L. Niu, D. Zhang, S. Ramakrishna, X. Zou, Recent advances in electrochemical cell-based biosensors for food analysis: strategies for sensor construction, Biosens. Bioelectron. 248 (2024) 115947, https://doi.org/10.1016/j.bios.2023.115947.

[4] D.M. Stanković, M. Jović, M. Ognjanović, A. Lesch, M. Fabián, H.H. Girault, B. Antić, Point-of-care amperometric determination of L-dopa using an inkjet-printed carbon nanotube electrode modified with dandelion-like MnO2 microspheres, Microchim. Acta 186 (2019), https://doi.org/10.1007/s00604-019-3644-x.

[5] E. Maiorano, S. Gianvittorio, M. Lanzi, D. Tonelli, H. Pick, A. Lesch, Print-light-synthesis of gold thin film electrodes for electrochemical sensing, Adv. Mater. Technol. 8 (2023), https://doi.org/10.1002/admt.202202039.

[6] Y. Zhou, Q. Wang, T. Xiang, X. Chen, Recent advances in electrochemical biosensors for bacterial detection, Nano TransMed. 4 (2025) 100078, https://doi.org/10.1016/j.ntm.2025.100078.

[7] M. Govindaraj, A. Srivastava, M.K. Muthukumaran, P.C. Tsai, Y.C. Lin, B.K. Raja, J. Rajendran, V.K. Ponnusamy, J.A. Selvi, Current advancements and prospects of enzymatic and non-enzymatic electrochemical glucose sensors, Int. J. Biol. Macromol. 253 (2023) 126680, https://doi.org/10.1016/j.ijbiomac.2023.126680.

[8] L.S. Guenang, L.M. Dongmo, S.L.Z. Jiokeng, A.T. Kamdem, G. Doungmo, I.K. Tonlé, V.C. Bassetto, M. Jović, A. Lesch, H. Girault, Montmorillonite clay-modified disposable ink-jet-printed graphene electrode as a sensitive voltammetric sensor for the determination of cadmium(II) and lead(II), SN Appl. Sci. 2 (2020), https://doi.org/10.1007/s42452-020-2283-5.

[9] D.V. Estrada-Osorio, R.A. Escalona-Villalpando, A. Gutiérrez, L.G. Arriaga, J. Ledesma-García, Poly-L-lysine-modified with ferrocene to obtain a redox polymer for mediated glucose biosensor application, Bioelectrochemistry 146 (2022) 108147, https://doi.org/10.1016/j.bioelechem.2022.108147.

[10] W. Cao, H. Wang, X. Zhang, Y. Wang, X. Jin, A novel ruthenium-based biosensor for interference-free continuous glucose monitoring via one-step electropolymerization strategy, Talanta 301 (2026) 129282, https://doi.org/10.1016/j.talanta.2025.129282.

[11] J. Wang, L.D. Hutchins, Thin-layer electrochemical detector with a glassy carbon electrode coated with a base-hydrolyzed cellulosic film, Anal. Chem. 57 (1985) 1536–1541, https://doi.org/10.1021/ac00285a010.

[12] N. Alizadeh, A. Georgas, C. Argirusis, G. Sourkouni, N. Argirusis, Polymer coatings for electrochemical biosensors, Coatings 16 (2026) 164, https://doi.org/10.3390/coatings16020164.

[13] M. Zinggeler, S. Schär, F. Kurth, Printed antifouling electrodes for biosensing applications, ACS Appl. Mater. Interface. 14 (2022) 56578–56584, https://doi.org/10.1021/acsami.2c17557.

[14] Y. Wang, G. Nian, J. Kim, Z. Suo, Polyacrylamide hydrogels. VI. Synthesis-property relation, J. Mech. Phys. Solid. 170 (2023) 105099, https://doi.org/10.1016/j.jmps.2022.105099.

[15] R. Jarošová, S.E. McClure, M. Gajda, M. Jović, H.H. Girault, A. Lesch, M. Maiden, C. Waters, G.M. Swain, Inkjet-printed carbon nanotube electrodes for measuring pyocyanin and uric acid in a wound fluid simulant and culture Media, Anal. Chem. 91 (2019) 8835–8844, https://doi.org/10.1021/acs.analchem.8b05591.

[16] D. Chan, J.C. Chien, E. Axpe, L. Blankemeier, S.W. Baker, S. Swaminathan, V. A. Piunova, D.Y. Zubarev, C.L. Maikawa, A.K. Grosskopf, J.L. Mann, H.T. Soh, E. A. Appel, Combinatorial polyacrylamide hydrogels for preventing biofouling on implantable biosensors, Adv. Mater. 34 (2022), https://doi.org/10.1002/adma.202109764.

[17] A.I. Jacobs, M.C. Prete, A. Lesch, A.A. Sebio, C.R. Teixeira Tarley, G.M. Swain, Measurement of Human and bovine exhaled breath condensate pH using polyaniline-modified flexible inkjet-printed nanocarbon electrodes, ACS Omega 9 (2024) 40841–40856, https://doi.org/10.1021/acsomega.4c05800.

[18] X. Xu, S. Lu, Z. Zhang, Hydrogel/MOF dual-modified photoelectrochemical biosensor for antibiofouling and biocompatible dopamine detection, Langmuir 40 (2024) 10718–10725, https://doi.org/10.1021/acs.langmuir.4c00727.

[19] Y. Zhang, Q. Xu, F. Wang, T. Gao, T. Wei, Enzyme powered self-assembly of hydrogel biosensor for colorimetric detection of metabolites, Sens. Actuat., B 375 (2023) 132942, https://doi.org/10.1016/j.snb.2022.132942.

[20] B. Amsden, Solute diffusion in hydrogels. An examination of the retardation effect, Polym. Gel. Netw. 6 (1998) 13–43, https://doi.org/10.1016/S0966-7822(97)00012-9.

[21] W.B.V. de Oliveira, G.C. da Silva, M.C.D.O. Leite, C.C. de Souza, T.P. Lisboa, M.A. C. Matos, R.C. Matos, Hydrogel-based electrochemical cells for carbendazim analysis using a miniaturized sensor, Electrochim. Acta 537 (2025) 146830, https://doi.org/10.1016/j.electacta.2025.146830.

[22] Y. Hiruta, Poly(N-isopropylacrylamide)-based temperature- and pH-responsive polymer materials for application in biomedical fields, Polym. J. 54 (2022) 1419–1430, https://doi.org/10.1038/s41428-022-00687-z.

[23] J. Liu, L. Jiang, S. He, J. Zhang, W. Shao, Recent progress in PNIPAM-based multi-responsive actuators: a mini-review, Chem. Eng. J. 433 (2022) 133496, https://doi.org/10.1016/j.cej.2021.133496.

[24] A. Das, A. Babu, S. Chakraborty, J.F.R. Van Guyse, R. Hoogenboom, S. Maji, Poly (N-isopropylacrylamide) and its copolymers: a review on recent advances in the areas of sensing and biosensing, Adv. Funct. Mater. 34 (2024), https://doi.org/10.1002/adfm.202402432.

[25] S. Lanzalaco, J. Mingot, J. Torras, C. Alemán, E. Armelin, Recent advances in poly (N-isopropylacrylamide) hydrogels and derivatives as promising materials for biomedical and engineering emerging applications, Adv. Eng. Mater. 25 (2023), https://doi.org/10.1002/adem.202201303.

[26] B. Mutharani, P. Ranganathan, S.M. Chen, Temperature-reversible switched antineoplastic drug 5-fluorouracil electrochemical sensor based on adaptable thermo-sensitive microgel encapsulated PEDOT, Sens. Actuat., B 304 (2020) 127361, https://doi.org/10.1016/j.snb.2019.127361.

[27] B. Mutharani, P. Ranganathan, S.M. Chen, H.C. Tsai, Temperature-responsive voltammetric sensor based on stimuli-sensitive semi-interpenetrating polymer network conductive microgels for reversible switch detection of nitrogen mustard analog chlorambucil (Leukeran™), Electrochim. Acta 374 (2021) 137866, https://doi.org/10.1016/j.electacta.2021.137866.

[28] T. Zhan, H. Xie, J. Mao, S. Wang, Y. Hu, Z. Guo, Conductive PNIPAM/CMCS/MWCNT/PANI hydrogel with temperature, pressure and pH sensitivity, ChemistrySelect 6 (2021) 4229–4237, https://doi.org/10.1002/slct.202101003.

[29] X. Dan, L. Ruiyi, W. Qinsheng, Y. Yongqiang, W. Guangli, L. Zaijun, Thermal-switchable sensor based on palladium-graphene composite and poly(N-isopropylacrylamide) for electrochemical detection of 4-nitrophenol, Microchem. J. 172 (2022) 106970, https://doi.org/10.1016/j.microc.2021.106970.

[30] P. Gwardys, K. Marcisz, D. Jagleniec, J. Romanski, M. Karbarz, Electroactive and thermoresponsive hybrid microgel on a gold surface for electrochemically controlled release of active substance, ACS Appl. Mater. Interface. 17 (2025) 36469–36477, https://doi.org/10.1021/acsami.5c06165.

[31] M. Sawicka, K. Marcisz, J. Romański, M. Strawski, O. Smutok, M. Gonchar, E. Katz, K. Kaniewska, M. Karbarz, A thermosensitive α-amino acid hydrogel layer deposited on an electrode surface: actuator and sensor performance, Talanta 296 (2026) 128454, https://doi.org/10.1016/j.talanta.2025.128454.

[32] Z. Yang, X. Yan, B. Xu, Z. Wang, Y. Wang, Precisely writing/printing hydrogel patterns on polymer surfaces, Chem. Eng. J. 485 (2024) 149851, https://doi.org/10.1016/j.cej.2024.149851.

[33] A. Lesch, F. Cortés-Salazar, V. Amstutz, P. Tacchini, H.H. Girault, Inkjet printed nanohydrogel coated carbon nanotubes electrodes for matrix independent sensing, Anal. Chem. 87 (2015) 1026–1033, https://doi.org/10.1021/ac503748g.

[34] S. Gianvittorio, M. Malferrari, H. Pick, S. Rapino, A. Lesch, Print-light-synthesis of ruthenium oxide thin film electrodes for electrochemical sensing applications, Bioelectrochemistry 163 (2025) 108909, https://doi.org/10.1016/j.bioelechem.2025.108909.

[35] S. Gianvittorio, D. Tonelli, A. Lesch, Print-light-synthesis for single-step metal nanoparticle synthesis and patterned electrode production, Nanomaterials 13 (2023) 1915, https://doi.org/10.3390/nano13131915.

[36] F. Weyand, S. Gianvittorio, F. Longo, J. Wang, A. Lesch, Switching between boosting and suppression of sensitivity and selectivity of inkjet-printed graphene electrodes for biomolecule detection, Electrochim. Acta 526 (2025) 146174, https://doi.org/10.1016/j.electacta.2025.146174.

[37] X. Yin, A.S. Hoffman, P.S. Stayton, Poly(N-isopropylacrylamide-co-propylacrylic acid) copolymers that respond sharply to temperature and pH, Biomacromolecules 7 (2006) 1381–1385, https://doi.org/10.1021/bm0507812.

[38] S. Ilić-Stojanović, M. Urošević, L. Nikolić, D. Petrović, J. Stanojević, S. Najman, V. Nikolić, Intelligent poly(N-isopropylmethacrylamide) hydrogels: synthesis, structure characterization, stimuli-responsive swelling properties, and their radiation decomposition, Polym. (Basel) 12 (2020) 1112, https://doi.org/10.3390/POLYM12051112.

[39] M.H. Pournaghi-Azar, R. Ojani, Catalytic oxidation of ascorbic acid by some ferrocene derivative mediators at the glassy carbon electrode. Application to the voltammetric resolution of ascorbic acid and dopamine in the same sample, Talanta 42 (1995) 1839–1848, https://doi.org/10.1016/0039-9140(95)01638-4.

[40] T.E. Lin, A. Lesch, C.L. Li, H.H. Girault, Mapping the antioxidant activity of apple peels with soft probe scanning electrochemical microscopy, J. Electroanal. Chem. 786 (2017) 120–128, https://doi.org/10.1016/j.jelechem.2017.01.015.